Self-Assembly of Large and Small Molecules into Hierarchically Ordered Sacs and Membranes
Ramille M. Capito, *et al.*
Science **319**, 1812 (2008);
DOI: 10.1126/science.1154586

34. E. Peik *et al.*, http://arxiv.org/abs/physics/0611088v1.
35. We thank C. W. Oates, M. A. Lombardi, and D. R. Smith for comments on the manuscript and K. Feder, J. Nicholson, and P. Westbrook for specialty nonlinear fiber used in the fiber frequency comb. This work was supported by the Office of Naval Research, Disruptive Technology Office, and NIST. P.O.S. acknowledges support from the Alexander von Humboldt Foundation. This work is a contribution of NIST and is not subject to U.S. copyright.

Supporting Online Material
www.sciencemag.org.cgi/content/full/1154622/DC1
SOM Text
Figs. S1 and S2
References

26 December 2007; accepted 20 February 2008
Published online 6 March 2008;
10.1126/science.1154622
Include this information when citing this paper.

Self-Assembly of Large and Small Molecules into Hierarchically Ordered Sacs and Membranes

Ramille M. Capito,[1] Helena S. Azevedo,[1,2] Yuri S. Velichko,[3] Alvaro Mata,[1] Samuel I. Stupp[1,3,4,5]*

We report here the self-assembly of macroscopic sacs and membranes at the interface between two aqueous solutions, one containing a megadalton polymer and the other, small self-assembling molecules bearing opposite charge. The resulting structures have a highly ordered architecture in which nanofiber bundles align and reorient by nearly 90° as the membrane grows. The formation of a diffusion barrier upon contact between the two liquids prevents their chaotic mixing. We hypothesize that growth of the membrane is then driven by a dynamic synergy between osmotic pressure of ions and static self-assembly. These robust, self-sealing macroscopic structures offer opportunities in many areas, including the formation of privileged environments for cells, immune barriers, new biological assays, and self-assembly of ordered thick membranes for diverse applications.

The organization of molecules at interfaces has been a phenomenon of great interest over the past few decades given its importance in the preparation of chemically defined surfaces and ordered materials. One classical system is the Langmuir-Blodgett film in which molecules are ordered by compression at an air-water interface, followed by deposition of multilayers through repeated immersion of a solid substrate into the liquid phase (*1*–*3*). Another widely studied system is the self-assembling monolayer formed at a solid-liquid interface by the reaction and self-ordering of dissolved molecules on a solid surface (*4*, *5*). Other systems include the formation of molecular complexes or solid objects at the interface of two immiscible liquids (*6*, *7*), and electrostatic layer-by-layer deposition of amorphous polymers at the solid-liquid interface through alternation of their charge (*8*).

We report the self-assembly of ordered materials well beyond the monolayer scale at an aqueous liquid-liquid interface. We combined a 1 to 2 weight (wt) % peptide amphiphile (PA) solution with a 0.5 to 2 wt% solution of the high molecular weight polysaccharide hyaluronic acid (HA) (fig. S1A). PAs are small synthetic molecules containing typically a hydrophobic alkyl segment covalently grafted to a short peptide. The one used here consisted of an alkyl tail of 16 carbons attached to the peptide sequence $V_3A_3K_3$ (fig. S1B). We previously developed a broad class of PAs that are known to self-assemble into high aspect ratio nanofibers (*9*–*11*). Their tolerance of arbitrary domains past a β-sheet–forming sequence makes them useful in biological signaling (*12*, *13*). HA is a linear negatively charged macromolecule containing a disaccharide repeat unit of *N*-acetylglucosamine and glucuronic acid, present in mammalian extracellular matrix. When PA and HA solutions were combined in equal volumes, we observed the immediate formation of a solid membrane localized at the interface between the two liquids. If the denser HA solution is placed on top of the PA solution, the HA fluid sinks into the PA component, causing renewal of the liquid-liquid interface and resulting in continuous growth of membrane until the entire volume of HA solution is engulfed (Fig. 1A). This leads to the formation of a polymer-filled sac over periods of minutes to hours depending on the volume and density of the liquids used. Alternatively, closed sacs can be made instantly by injecting one solution directly into the bulk of the other, creating either HA-filled or PA-filled sacs. Other PAs tested led to similar results without obvious kinetic differences. However, as expected, the nature of the peptide sequence does affect the structural integrity of the membranes formed.

The instant initiation of ordered structures allows formation of self-sealing sacs (Fig. 1, B to D), films with tailorable size and shape (Fig. 1E), as well as continuous strings (Fig. 1F). Confocal microscopy confirmed the incorporation of both HA and PA components within the sac membranes (Fig. 1, G to I). Although formation of solids between oppositely charged macromolecules has been widely demonstrated (*14*–*17*), these systems commonly produce dense and disordered materials that are not permeable to large molecules (e.g., proteins) and are unstable in water without the use of cross-linking chemistry. Moreover, a large defect such as a hole or a crack in a solid made up of two oppositely charged polymers cannot be rapidly repaired by diffusion. The highly ordered materials described here are mechanically robust in both dry and hydrated states, can be permeable to proteins, and have the capability to self-seal defects instantly by self-assembly.

Recognizing the importance of electrostatic charge screening on the self-assembly of PA nanofibers, we investigated the effect of zeta potential in HA and PA solutions on membrane formation (*18*). Sac membranes with physical integrity formed only when both solutions had strong zeta potentials of opposite charge (Fig. 1J). The zeta potential determines the degree of stability of charged aggregates in solution, and in this case should correlate to the total electrostatic charge of molecules in the presence of counterions.

We investigated the microstructure of the PA-HA sac membranes as a function of time using electron microscopy (EM) (*18*). In the early stages of liquid-liquid contact, scanning electron micrographs reveal an amorphous layer (Fig. 2, A and D, region 1) adjacent to a layer of parallel fibers on the PA solution side (Fig. 2, A and D, region 2). We believe that rapid diffusion of the small PA molecules into the HA solution and electrostatic complexation of both molecules result in the formation of the amorphous zone. The parallel fiber region, which measures ~150 nm within 1 min of contact, is the result of self-assembly triggered by electrostatic screening of the amphiphiles by the negatively charged HA molecules near the interface. These early events that occur upon contact between the two liquids establish a diffusion barrier, which prevents the rapid mixing of the two miscible liquids. Ordered growth of nanofibers oriented perpendicular to the interface then forms a layer that measures ~1.5 μm after 30 min (Fig. 2B, region 3) and ~20 μm after 4 days of initial contact (Fig. 2C, region 3).

Transmission electron microscopy (TEM) of cross-sectional slices of a hydrated membrane sample (Fig. 2, E and F) (*18*) confirmed the morphologies observed by scanning electron microscopy (SEM) (Fig. 2D). TEM revealed the presence of the high–molar mass polymer throughout the

[1]Institute for BioNanotechnology in Medicine, Northwestern University, Chicago, IL 60611, USA. [2]3B's Research Group, Biomaterials, Biodegradables and Biomimetics, Department of Polymer Engineering, University of Minho, Braga, Portugal. [3]Department of Materials Science and Engineering, Northwestern University, Evanston, IL 60208, USA. [4]Department of Chemistry, Northwestern University, Evanston, IL 60208, USA. [5]Department of Medicine, Northwestern University, Chicago, IL 60611, USA.

*To whom correspondence should be addressed. E-mail: s-stupp@northwestern.edu

thickness of the membrane (dark regions indicate positive staining of HA by uranyl acetate). The parallel fiber region between the amorphous layer and the perpendicular fibers is more obvious in the TEM micrographs (Fig. 2E, region 2). We calculated the HA density across the membrane shown in Fig. 2E by image analysis (Fig. 2G). The density profile shows three independent regions: (1) a region with an approximately constant polymer density, (2) a region of parallel fibers where there is a maximum in polymer density, and (3) a region of perpendicular fibers where the polymer density decays with increasing distance from the amorphous region. Most of region 1, where there is constant HA density, is probably excess HA from the bulk solution that is merged with a portion of the amorphous region of the membrane. The observed accumulation of HA component in the region of parallel oriented nanofibers (Fig. 2E, region 2) suggests a denser arrangement of nanostructures in that zone. We expect that diffusion of both the large and small molecules will eventually slow down as density increases in the perpendicular fiber region. This is supported by the decrease in HA density across the region of perpendicular fibers.

The mechanical properties of PA-HA membranes were evaluated by a tensile test (*18*). The elastic moduli in the dry and hydrated states of the membrane were found to be about 670 and 0.9 MPa, respectively (Fig. 3A). For comparison, we measured the moduli of membranes formed by the complexation of two oppositely charged polysaccharides, chitosan and gellan (both of high molecular weight). The combination of these two polysaccharides has been previously shown to form macroscopic capsules and strings (*15*, *17*), thus serving as a suitable comparison to our self-assembling systems. The elastic modulus of PA-HA membranes was found to be about nine times higher than that of the chitosan-gellan membranes in both hydrated and dry states (Fig. 3A). Despite their lower stiffness, SEM micrographs of the chitosan-gellan membranes (Fig. 3C) showed a dense structure compared to the PA-HA membrane (Fig. 3B). Furthermore, the chitosan-gellan membranes, swollen to about 20 times their original dry thickness, behave more like hydrogels and fall apart over time when immersed in water. Hydrated PA-HA membranes, in contrast, exhibit minimal dimensional change and remain very stable over months in either water or phosphate-buffered saline. We conclude that hierarchical order contributes to their greater hydrolytic stability and robust mechanical properties.

We found that it is possible to reseal a macroscopic hole in a polymer-filled sac. Using a diacetylene PA molecule (fig. S2) that can be polymerized after self-assembly to an intense blue color (*19*), we were able to create HA-filled sacs in which a macroscopic defect can be easily visualized (Fig. 3D). Because the HA component was contained within the sac, application of additional PA solution within the defect space created a new membrane segment with edges sufficiently sealed to the original sac membrane to prevent leakage of the fluid inside (Fig. 3E). Sealing of the defect does not require polymerization of the PA molecules. Nonetheless, in this case, PA molecules in the repaired region were polymerized to match the appearance of the original sac membrane. Because of their robust character, the PA-HA sacs can also be easily manipulated and sutured (Fig. 3F). When sutured, the sac can hold its own weight without further tearing of the membrane (Fig. 3G).

A common limitation of polyelectrolyte complexes is lack of permeability to larger molecules such as proteins and nucleic acids. We therefore tested the permeability capabilities of the PA-HA membrane by monitoring diffusion of transforming growth factor–β1 (TGF-β1, 25 kD) out of a PA gel-filled sac (*18*). As a control in this experiment, a PA gel was created without the surrounding sac membrane. Sacs enclosing a PA gel and TGF-β1 were created by mixing an ~1 wt% negatively charged PA (fig. S3) and TGF-β1 (2 ng per sac) with the HA solution before injecting the mixture into the positively charged PA. To subsequently gel the negative PA inside, we placed an aliquot of calcium chloride solution on top of the sac, which penetrates the membrane and triggers self-assembly of the negatively charged PA. Results over a 2-week period revealed similar TGF-β1 release kinetics between the gels with and without the surrounding membrane structure (Fig. 3H), thus confirming the permeability of the HA-PA membrane to proteins.

To investigate if these PA-HA structures can support cell viability and differentiation, we performed in vitro studies using human mesenchymal stem cells (hMSCs) (*18*). Expanded hMSCs were incorporated within gel-filled sacs and cultured in growth media, growth media supplemented with TGF-β1, chondrogenic media, or chondrogenic media supplemented with TGF-β1. The hMSCs remained viable within the sacs (Fig. 3I) for up to 4 weeks in culture. Furthermore, results obtained with real-time reverse transcription polymerase chain reaction after 2 weeks in culture (Fig. 3J) revealed an increase in collagen type II gene expression when cells in sacs were stimulated with TGF or chondrogenic media, indi-

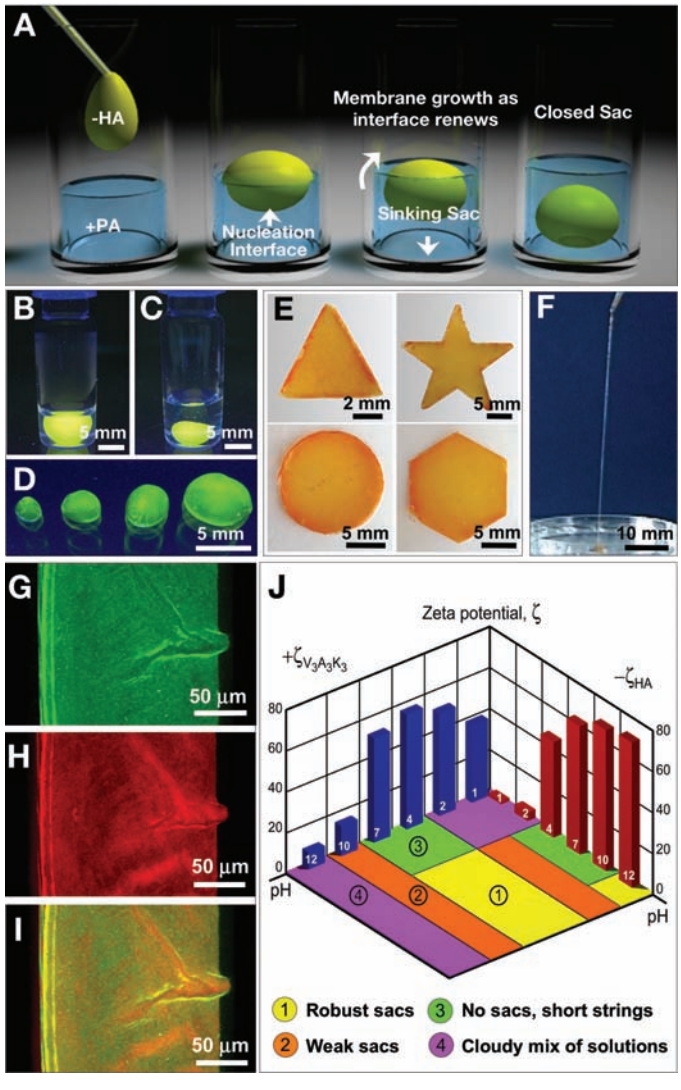

Fig. 1. (**A**) Schematic representation of one method to form a self-sealing closed sac. A sample of the denser negatively charged biopolymer solution is dropped onto a positively charged peptide amphiphile (PA) solution. (**B**) Open and (**C**) closed sac formed by injection of a fluorescently tagged hyaluronic acid (HA) solution into a PA solution. (**D**) Self-assembled sacs of varying sizes. (**E**) PA-HA membranes of different shapes created by interfacing the large- and small-molecule solutions in a very shallow template (~1 mm thick). (**F**) Continuous strings pulled from the interface between the PA and HA solutions. (**G** to **I**) Confocal microscopy of the fluorescein-labeled HA component (G) and the rhodamine-labeled PA (H) within the sac membrane. (I) Merged images demonstrate colocalization of the PA and HA molecules within the membrane. (**J**) Zeta potential measurements of HA and PA solutions measured over a wide range of pH values with a qualitative rating assessing the ability to form well-defined sac structures at each pH condition.

cating that hMSCs were able to differentiate toward a chondrogenic phenotype within the sacs. The self-assembling sacs could therefore provide sufficient nutrient diffusion necessary for cell survival and differentiation.

We have formulated a possible mechanism for the self-assembly of these hierarchically ordered structures. Upon liquid-liquid contact, we first expect rapid mixing by diffusion of molecules localized at the interface (Fig. 4A), with the small molecules diffusing readily into the polymer solution and leading to electrostatic complexation. Ionic screening along the entire contact area leads simultaneously to self-assembly of PA nanofibers localized at the interface (Fig. 4B). This creates a diffusion barrier for long entangled HA chains and PA molecules or their aggregates, resulting in the physical separation of both components. Subsequent growth of fibers oriented perpendicular to the interface occurs toward the PA side as indicated by electron microscopy. This suggests that the megadalton macromolecules diffuse into the small-molecule solution. At first glance this is counterintuitive because one might expect the small molecules to diffuse more rapidly into the polymer solution. Diffusion of the large macromolecules into the PA solution, however, can be driven by the osmotic pressure imbalance between the PA and HA solutions. This imbalance is primarily due to the preservation of macroscopic electroneutrality; because of the greater charge density in a high molecular weight polyelectrolyte, a greater number of ions are required to neutralize the total charge in the HA solution compared to the PA solution. This difference in ion concentration results in an excess osmotic pressure of ions in the HA compartment, resulting in reptation of macromolecules through the diffusion barrier. These macromolecules entering the PA side could then nucleate PA nanofibers perpendicular to the contact interface (Fig. 4C).

By applying Poisson-Boltzman theories to the cell model of polyelectrolytes (*20*, *21*), one can describe the difference in osmotic pressure $\Delta\Pi$ between the two solutions by the expression

$$\Delta\Pi \equiv \Pi_{HA} - \Pi_{PA} = k_B T \sum_i n_i \left(e^{-\frac{e\nu_i \psi(R)}{k_B T}} - 1 \right)$$

where n_i and ν_i are the concentration and valence of mobile ions, $\psi(R)$ is a local electrostatic potential, R is the Wigner cell radius, k_B is the Bolzmann constant, and T is the temperature (*20*). The electrostatic potential is proportional to the measured zeta potential, ζ, in our earlier experiments and has a direct effect on the osmotic pressure difference as follows:

$$\Delta\Pi \sim \zeta^2 \sum_i \frac{n_i (e\nu_i)^2}{2k_B T} \geq 0$$

Therefore, a substantial difference in zeta potential between the two components will result in a large difference in osmotic pressure. Under excess osmotic pressure in the HA compartment, macromolecules will preferentially diffuse through the initially formed contact layer. The required elongated conformation of the HA molecule for diffusion through the pores of the contact layer also creates an entropic barrier that can be overcome only when the excess osmotic pressure dominates. The diffusion driven by the excess osmotic pressure, $\Delta\Pi$, can be described by the Smoluchowski equation

$$\frac{\partial}{\partial t} w(s,t) = D_o \frac{\partial}{\partial s} \left[\frac{\partial}{\partial s} + \frac{\Delta\Pi \lambda b^2 - F}{k_B T} \right] w(s,t)$$

where D_o is the bare diffusion coefficient, λ is the thickness of the diffusive barrier, b is the HA monomer size, $F \propto k_B T \ln(N - s)$ is the entropic free energy of a polymer chain of N repeats with s monomer units that have passed through the membrane, and $w(s,t)$ determines the probability of having a segment of s monomers at time t through the membrane. The released free ends of HA molecules, after complete reptation through the contact layer, produce polymer "stubs" at the surface of the contact layer (Fig. 4D) that attract the oppositely charged PA molecules (Fig. 4B) and nucleate the self-assembly of perpendicularly oriented nanofibers through electrostatic screening (Fig. 4C). Growth of the nanofibers would then occur by attraction of PA aggregates at the base of the polymer stubs as "new" HA segments continue to penetrate through the parallel fiber mesh (Fig. 4, C and E). Self-assembly of the hybrid nanofibers should release condensed counterions that subsequently migrate to the polymer side, given the high affinity of polyelectrolytes for small ions. Hence, the excess osmotic pressure difference can be sustained in a dynamic fashion to continuously pump additional polymer chains through the barrier. One would expect that extensive self-assembly and elongation of these fibers would lead to a crowding effect that further increases the orientational order or align-

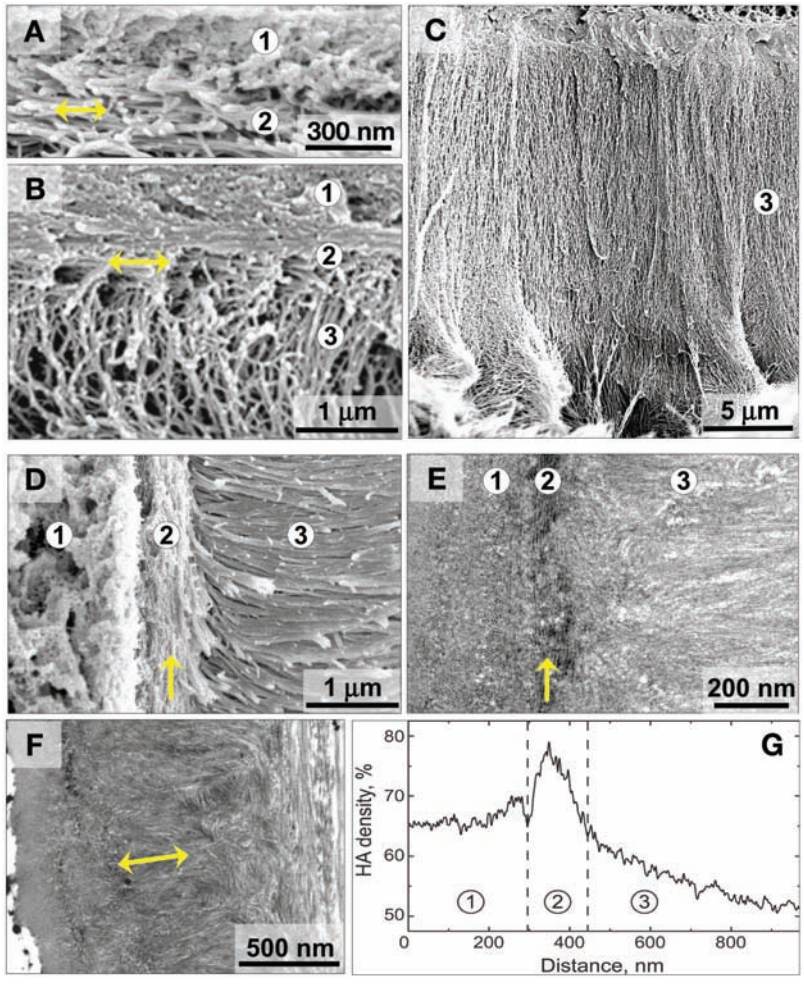

Fig. 2. (**A** to **C**) SEM of the sac membrane as it forms over time (HA solution side on top, PA solution side on bottom): (A) 1 min, (B) 30 min, and (C) 4 days. TEM of a cross-sectional slice of the membrane (**E** and **F**) show morphologies similar to those observed in SEM (**D**), particularly the perpendicularly oriented nanofibers (F, arrows). The parallel fiber region (arrow) between the amorphous and perpendicular fiber zones is most obvious in TEM (E, region 2). Dark regions indicate positive staining of HA by uranyl acetate. (**G**) Polymer density profile obtained by image analysis of (E) quantifying the density of dark regions across the membrane.

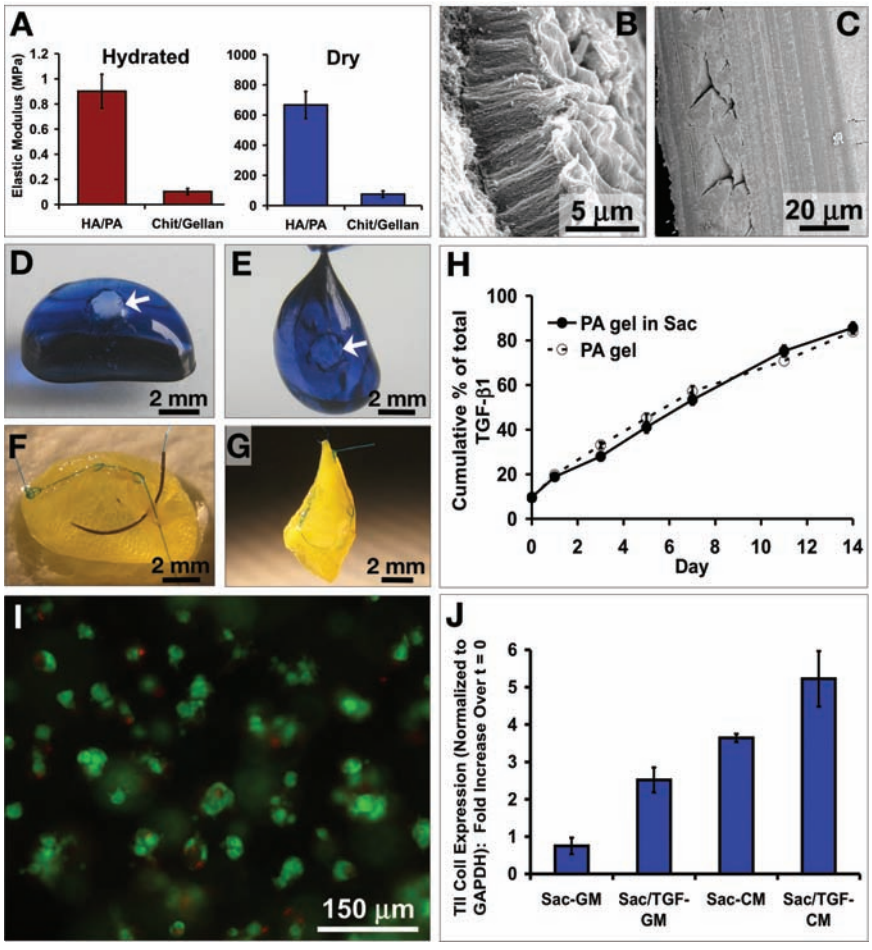

Fig. 3. (**A**) Tensile test data comparing the elastic modulus of the self-assembled membrane to an amorphous membrane composed of chitosan and gellan in both the dry and hydrated states. (**B** and **C**) SEM showing the cross sections of (B) the hierarchically ordered membrane and (C) the amorphous polymer-polymer membrane [the striations in (C) are effects from slicing the dense membrane during sample preparation]. (**D**) Hierarchically ordered sac formed with polydiacetylene PA containing a macroscopic defect within the membrane (arrow). (**E**) Sac in (D) after the defect is repaired and the sac resealed by triggering additional self-assembly with a drop of PA (arrow). Sacs are robust enough to withstand suturing (**F**) and can hold their weight without further tearing of the membrane (**G**). (**H**) TGF-β1 release from PA gel-filled sacs and PA gels as a function of time, demonstrating a nearly identical protein-release profile. (**I**) Live/dead assay of hMSCs cultured within the PA gel-filled sacs (green cells are live, red cells are dead) showing that most of the cells remain viable. (**J**) Collagen type II gene expression of hMSCs cultured within the PA gel–filled sacs in growth medium (GM), growth medium supplemented with TGF-β1 (TGF-GM), chondrogenic medium (CM), and chondrogenic medium supplemented with TGF-β1 (TGF-CM). Error bars in (A), (H), and (J) denote SD.

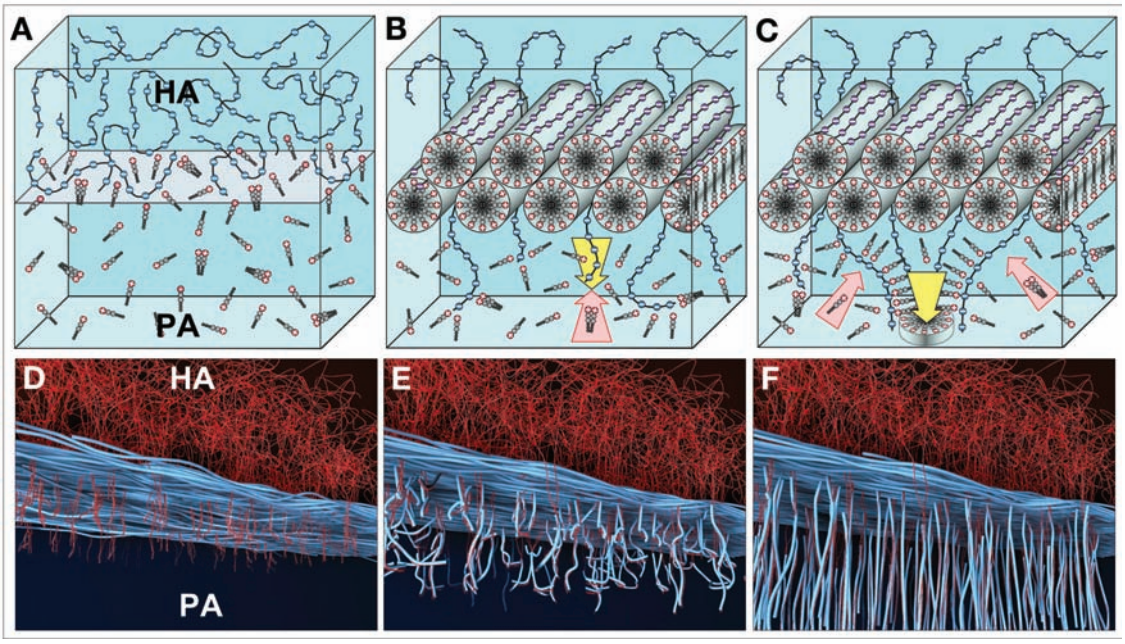

Fig. 4. (**A** to **F**) Schematic illustration of the proposed model for ordered PA-HA membrane formation. (A) Initial mixing of the large and small molecules at the interface. (B) Formation of nanofibers at the interface composed of small molecules (due to electrostatic screening by the negatively charged polymer) creates a physical barrier between the two solutions. This is followed by reptation of macromolecules through the barrier and into the small-molecule solution (yellow arrow). (C) Nucleation of nanofibers perpendicular to the interface by polymer strands crossing the barrier (yellow arrow). Pink arrows indicate attraction of PA monomer or their aggregates to polymer strands as they continue to cross the barrier. (D) Schematic representation of polymer stubs (red) penetrating the diffusion barrier. (E) Subsequent self-assembly of nanofibers (blue) initiated by the stubs. These nanofibers start gaining orientation perpendicular to the interface as polymer diffuses further into the small-molecule solution. (F) Growth of the nanofibers perpendicular to the interface over time, becoming denser and increasingly aligned as the membrane thickens.

ment in this region over time (Fig. 4F), as demonstrated earlier by microscopy (Fig. 2C).

The synergistic interaction between large and self-assembling small molecules with both static and dynamic components has great potential for the discovery of highly functional materials. The sacs formed by these self-assembling systems could be attractive controlled environments for cells in assays or therapies. Moreover, ordered thick membranes could be molecularly customized to possess desired physical or bioactive functions. An interesting possibility is to design similar systems in organic solvents for nonbiological applications.

References and Notes

1. K. B. Blodgett, *J. Am. Chem. Soc.* **57**, 1007 (1935).
2. H. Ringsdorf, B. Schlarb, J. Venzmer, *Angew. Chem. Int. Ed. Engl.* **27**, 114 (1988).
3. J. A. Zasadzinski, R. Viswanathan, L. Madsen, J. Garnaes, D. K. Schwartz, *Science* **263**, 1726 (1994).
4. C. D. Bain *et al.*, *J. Am. Chem. Soc.* **111**, 321 (1989).
5. G. M. Whitesides, P. E. Laibinis, *Langmuir* **6**, 87 (1990).
6. L. Pirondini *et al.*, *Proc. Natl. Acad. Sci. U.S.A.* **99**, 4911 (2002).
7. N. Bowden, A. Terfort, J. Carbeck, G. M. Whitesides, *Science* **276**, 233 (1997).
8. G. Decher, *Science* **277**, 1232 (1997).
9. J. D. Hartgerink, E. Beniash, S. I. Stupp, *Science* **294**, 1684 (2001).
10. H. A. Behanna, J. J. J. M. Donners, A. C. Gordon, S. I. Stupp, *J. Am. Chem. Soc.* **127**, 1193 (2005).
11. K. Rajangam *et al.*, *Nano Lett.* **6**, 2086 (2006).
12. G. A. Silva *et al.*, *Science* **303**, 1352 (2004).
13. H. Storrie *et al.*, *Biomaterials* **28**, 4608 (2007).
14. S. Wen, Y. Xiaonan, W. T. K. Stevenson, *Biomaterials* **12**, 374 (1991).
15. H. Yamamoto, Y. Senoo, *Macromol. Chem. Phys.* **201**, 84 (2000).
16. H. Yamamoto, C. Horita, Y. Senoo, A. Nishida, K. Ohkawa, *J. Appl. Polym. Sci.* **79**, 437 (2001).
17. K. Ohkawa, T. Kitagawa, H. Yamamoto, *Macromol. Mater. Eng.* **289**, 33 (2004).
18. Materials and methods are available as supporting material on *Science* Online.
19. L. Hsu, G. L. Cvetanovich, S. I. Stupp, *J. Am. Chem. Soc.* 10.1021/ja076553s (2008).
20. M. Deserno, H. H. von Grunberg, *Phys. Rev. E Stat. Nonlin. Soft Matter Phys.* **66**, 011401 (2002).
21. C. Holm, P. Kékicheff, R. Podgornik, *Electrostatic Effects in Soft Matter and Biophysics* (NATO Science Series II, Kluwer, Dordrecht, Netherlands, 2001), pp. 27–52.

22. Supported by the U.S. Department of Energy (grant DE-FG02-00ER45810), the NIH (grants 5-R01-EB003806, 5-R01-DE015920, and 5-P50-NS054287), and the NSF (grant DMR-0605427). We thank N. A. Shah for the suturing tests, L. Hsu for synthesis of the diacetylene peptide amphiphile, R. Walsh for processing TEM samples, the Brinson laboratory at Northwestern University for assistance with mechanical testing, and M. Seniw for assistance with illustrations.

Supporting Online Material

www.sciencemag.org/cgi/content/full/319/5871/1812/DC1
Materials and Methods
Figs. S1 to S3

26 December 2007; accepted 7 February 2008
10.1126/science.1154586

The Transition from Stiff to Compliant Materials in Squid Beaks

Ali Miserez,[1,2,3] Todd Schneberk,[2,3] Chengjun Sun,[2,3] Frank W. Zok,[1]* J. Herbert Waite[2,3]*

The beak of the Humboldt squid *Dosidicus gigas* represents one of the hardest and stiffest wholly organic materials known. As it is deeply embedded within the soft buccal envelope, the manner in which impact forces are transmitted between beak and envelope is a matter of considerable scientific interest. Here, we show that the hydrated beak exhibits a large stiffness gradient, spanning two orders of magnitude from the tip to the base. This gradient is correlated with a chemical gradient involving mixtures of chitin, water, and His-rich proteins that contain 3,4-dihydroxyphenyl-L-alanine (dopa) and undergo extensive stabilization by histidyl-dopa cross-link formation. These findings may serve as a foundation for identifying design principles for attaching mechanically mismatched materials in engineering and biological applications.

Living organisms are functional assemblages of different interconnected tissues. Not infrequently, tissues with highly disparate mechanical properties (e.g., bone and cartilage, shell and adductor muscle, nail and skin) are joined together (*1*). In practice, the joining of dissimilar materials can lead to high interfacial stresses and contact damage (*2*, *3*). In apparent contradiction to this, the contacts between mechanically mismatched biomolecular tissues are remarkably robust. Mechanical-property gradients are increasingly invoked as the principal reason for their mechanical performance. The dentino-enamel junction (*4*), arthropod exoskeleton (*5*), polychaete jaws, and mussel byssal threads (*6*) all exhibit such gradients. Optical properties in squid eyes have also been correlated to a protein-density gradient (*7*). Although much is known about the mechanical and biochemical properties of the separate tissues, surprisingly little has been done to explain how mixtures of macromolecules are adapted for incremental mechanical effects at interfaces.

The beak of the Humboldt squid *Dosidicus gigas* is an example of a system with grossly mismatched tissues. It is composed of slightly offset apposing upper and lower parts that make no hard pivotal contact with one another and are set into a muscular buccal mass that controls their movement (*8*). The beak tip (or rostrum) is among the hardest and stiffest of wholly organic biomaterials (*9*). With a single notch through the thick dorsal integument of a captured fish, a squid beak can sever the nerve cord to paralyze prey for later leisurely dining (*10*). The predatory activity of a stiff razor-sharp beak embedded in a softer muscle mass might be compared to a person carving a roast with a bare metal blade. In both scenarios, there would be as much damage to self as to the intended objects. We found that the squid's task is facilitated by a beak design that incorporates large gradients in mechanical properties, intricately linked with local macromolecular composition, from the hard, stiff tip to the soft, compliant base.

When detached from the buccal mass, each Humboldt squid beak exhibits clearly visible gradients in pigmentation, ranging from translucent along the wing edge to black at the beak tip (Fig. 1, B and C). The pigmentation gradient appears to be closely coupled to a distribution of catechols that correspond to proteins containing 3,4-dihydroxyphenyl-L-alanine (dopa) (*9*). Catechol staining (red in Fig. 1D) is evident in the lightly tanned regions and more intensely (though largely obscured by black pigment) in the heavily tanned regions. Because the beaks are large enough to allow cutout specimens showing incremental differences in pigmentation (Fig. 1E), we performed coupled chemical and mechanical analyses to explore the consequences of pigmentation (figs. S1 and S2).

We carried out chemical analyses of consecutive cutouts after degradation by two treatments that preferentially attack different structural components: acid hydrolysis, which hydrolyzes protein and chitin but not the tanning pigment, and alkaline peroxidation, which solubilizes everything but chitin (see flowchart in fig. S1). The hydrolyzed untanned material is dominated by glucosamine, the basic structural unit of chitin [Fig. 2A(i)], whose presence was independently established by fiber x-ray diffraction (*9*). On the basis of glucosamine detection, chitin content in this region is estimated to be 90% of dry weight, compared to a low of 15 to 20% in the rostrum [Fig. 2A(ii)]. The amino acid composition of hydrolysates from all tanned regions is uniform and dominated by Gly, Ala, His and Asx (where Asx represents Asp and Asn combined) (27, 15, 11, and 7 mole percent, respectively) (Fig. 2, A and B). Only the untanned region differed in composition, with the Asx content being considerably higher and that of the other amino acids being somewhat lower than the corresponding values in the tanned regions. This disparity may

[1]Materials Department, University of California, Santa Barbara, CA 93106, USA. [2]Department of Molecular, Cellular, and Developmental Biology, University of California, Santa Barbara, CA 93106, USA. [3]Marine Science Institute, University of California, Santa Barbara, CA 93106, USA.

*To whom correspondence should be addressed. E-mail: zok@engineering.ucsb.edu (F.W.Z.); waite@lifesci.ucsb.edu (J.H.W.)